The Journal of the Korean Society of Oceanography
Vol. 30, No. 6, pp. 565-583, December 1995

A Numerical Study on the Interaction of Ulleung Warm Eddy with Topography and Lateral Boundary

Keun-Sik Lim and Kuh Kim*
Department of Oceanography, Korea Naval Academy
**Department of Oceanography, Seoul National University, Seoul 151-742, Korea*

울릉 난수성 Eddy와 해저지형과의 상호작용에 관한 수치모델 연구

임근식 · 김 구*
해군사관학교 해양학과, *서울대학교 자연과학대학 해양학과

We have used a nonlinear quasi-geostrophic model to study effects of lateral friction and bottom topography on the motion of warm eddies. The two empirical orthogonal functions of the stream function, accounting for the vertical structure, represent the barotropic and first baroclinic dynamic modes. This model is integrated 360 days on a 1000 km × 1000 km domain with a resolution of 10 km × 10 km including both the thermocline and idealized topography of the East Sea. Prescribed inflow through the Korea Strait is compensated by outflow through the Tsugaru Strait. The balance between the nonlinear advection term and the planetary β-effect tends to make northward movement of warm eddy over a flat bottom. The motion of a warm eddy over a sloping topography can be dominated by the nonlinear advection, while nonlinearity plays a secondary role over a flat topography. For eddies dispersing over topography, the nonlinear tendency is a function of time. For a strong warm eddy, northward propagation can occur. For intermediate strength of eddies one might expect a balance between the nonlinear term and the topographic β-effect. As nonlinearity decreases with eddy dispersion, southward motion along the slope may occur by such as a topographic Rossby wave. Our numerical simulations have confirmed the importance of lateral friction on eddy motions, in such a way that the northward penetration of the warm eddy increases drastically by the decrease of the lateral friction. The northward motion of warm eddy can be prevented by reducing the Reynolds number sufficiently. We have also demonstrated the crucial role of topographic effects in the eddy motion process.

난수성 eddy의 운동에 있어서 경계면 마찰과 해저지형의 중요성을 연구하기 위하여 비선형 QG-모델이 사용되었다. 수직구조를 나타내는 유선함수의 경험적 직교함수는 순압과 제 1 경압 역학 함수를 표현한다. 이 모델은 10 km × 10 km의 격자간격을 지닌 1000 km × 1000 km으로 구성되어 있고 360일동안 시험하였다. 대한해협을 통한 유입량은 쓰가루해협을 통하여 빠져 나간다. 울릉분지내(평평한 해저지형)에서는 QG 방정식의 비선형 이류항과 β-효과사이에 균형이 난수성 eddy를 북쪽으로 이동하게 한다. 대륙사면위에서의 난수성 eddy는 비선형항이 중요하게 작용하지만, 평평한 지형에서는 보조적인 역활을 한다. 해저지형이 변화하는 해역에서 난수성 eddy의 비선형항은 시간의 함수이다. 강한 eddy는 북쪽으로 이동한다. Eddy의 세기가 약해지면, 비선형항과 지형적인 베타효과항이 균형을 이루게 된다. Eddy의 분산과 함께 비선형성이 감소하므로서, 지형적 Rossby파 개념에 의하여 난수성 eddy는 대륙사면을 따라서 남하한다. 수치실험은 난수성 eddy의 운동에 미치는 경계면 마찰의 중요성을 확인하였다. 난수성 eddy의 북쪽 침투거리는 경계면 마찰계수의 감소로 증가하게 된다. 아울러 Reynolds number의 감소로 북쪽이동을 방지할 수 있다. 또한 이 난수성 eddy 운동과정에 있어서 해저지형이 중요한 역할을 하는 것이 제시되었다.

1. INTRODUCTION

Recent studies have shown that the Ulleung warm eddy plays an important role in the circulation of the East Sea (Tameishi, 1987; Ichiye and Takano, 1988; Na and Kim, 1990; Seung *et al.*, 1990; Kim, 1991; Kim *et al.*, 1991). The warm eddy is located in the central part of the Ulleung Basin where the local depth exceeds 1500 m (Kang and Kang, 1990). This warm eddy is quasi-circular, having a diameter of approximately 150 km (Fig. 1, Kim, 1991). When the warm eddy approaches the western slope of the East Sea, a large-scale northward flow developes in the upper layer near the coast of Korea according to Isoda and Saitoh (1993), who indicated that interaction between the warm eddy and neighboring synoptic warm water around Ulleung Basin has a strong influence on the movement of the intruding eddy and its structural change. This large anticyclonic eddy with diameters of 100 to 150 km is a major contributor to the mass transport in the northern part of the East Sea (Shin *et al.*, 1995). It is evident that behavior of warm eddy is important in understanding the circulation in the western part of the East Sea (An *et al.*, 1994).

This study investigates dynamical processes concerning the propagation and the formation of warm eddy through a series of numerical experiments similar to previous works by Wert and Reid (1972), Holland and Lin (1975), Hurlbert and Thompson (1980) and Sturges, *et al.* (1993). Wert and Reid (1972) considered a two-layer prognostic model of the circulation in the Gulf of Mexico. A one-year prediction was made of the baroclinic and barotropic modes of circulation in the Gulf forced by the inflow through the Yucatan Strait which varies seasonally. Hurlbert and Thompson (1980) proved that the reduced gravity model is the simplest model to simulate the basic dynamics of the mean current and the eddy generation. They also indicated that baroclinic instability is not an essential element of the dynamics because bottom topography plays an important role in steering eddies in the upper ocean.

Effects of eddy size and strength and bottom friction on the propagation and decay of the warm eddy have been well demonstrated in previous numerical investigations (McWilliams and Flierl, 1979; Smith and Reid, 1982; Smith and O'Brien, 1983; Smith, 1986). However, influences of lateral friction and bottom topography, which may be important in the dynamics of these features, remain to be investigated. Ulleung warm eddy have been observed to propagate onto continental slope and shelf regions(Kang and Kang, 1990). This study will seek to examine the basic dynamics of the warm eddy as influenced by a linearly sloping bottom topography.

A series of numerical experiments is designed to determine the response of anticyclonic eddies to topography and the western boundary of the East Sea. With this objective, several flat-bottom, quasi-geostrophic numerical experiments with different lateral frictions will be compared. Effects of eddy strength, lateral friction and location relative to topography on eddy motion and decay will be examined. In Section 2 the mathematical formulation of the problem is presented. In Section 3 effects of lateral friction and bottom topography on the Ulleung warm eddies will be examined.

2. MODEL FORMULATION AND PARAMETERS

In this study we use a quasi-geostrophic model with two empirical orthogonal functions (EOF) modes in the vertical structure. All physical and numerical parameters that define the principal numerical experiments presented in this study are given in Table 1. First we consider the vertical structure function for a realistic stratification. The mean Brunt-Väisälä frequency in the following numerical experiments (Fig. 2a) was estimated from the FRDA's data taken at Station 104-08 August, 1989. Values of the reduced gravity are chosen such that the base of the main thermocline lies at the depth of 300 m. The vertical eigenmodes, $F_n(z)$, associated with the stratification are shown in Fig. 2b. Mode F_0 is the barotropic one and the first two baroclinic modes (modes F_1 to F_2) are surface intensified.

Two mode representation of the stream function for this model may be accounted for by two EOF's

given in equation (1). The vertical structures associated with EOF modes E_1 and E_2 shown in Fig. 2c can be represented by the barotropic and the first baroclinic dynamic modes (F_0 and F_1) with a residual variance generally less than 10 percent. Empirical orthogonal functions in the time domain (e.g., Tang and Weisberg, 1988) were determined separately for each of the velocity components and the vertical displacement by solving for the eigenvalues and eigenvectors of their respective covariance matrices over ten record depths. They

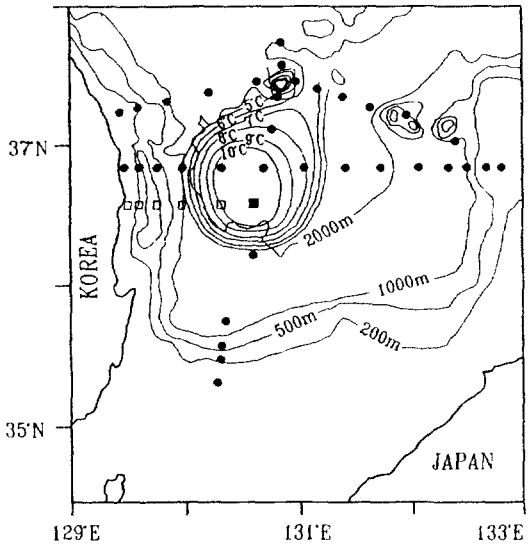

Fig. 1. Horizontal temperature distribution at 200m depth, 8~15 July 1989 from Kim (1991). Subsequent data (Kim, 1991) indicates that a warm eddy was formed by the Tsushima Warm Current during summer seasons.

Table 1. Model parameters for the standard case

A_H: Lateral friction coefficient ($=3\times10^{6}$ cm^{2}sec^{-1})	β: Latitude gradient of f ($=2\times10^{-13}$ cm^{-1}sec^{-1})
f_o: Variable Coriolis parameter ($=8.77\times10^{-5}$ sec^{-1})	τ_o: Wind stress ($=1.0\times10^{-8}$ dyne/cm^2)
g: gravity (=980 cm sec^{-2})	ρ: density (=1.0 gm^{-3})
Δx: grid space (=10 km)	Δy: grid space (=10 km)
Δt: time interval (=1 hr)	
r: Bottom friction coefficient ($=1\times10^{-7}$ s^{-1})	

Domain size, $L_x\times L_y$=1000 km$\times$1000 km
Korea Strait width L_4: 200 km
Tsugaru Strait width L_4: 100 km
Maximum inflow transport: 3×10^{6} m^3 sec^{-1}
Radius of deformation: 31.2 km
Wind pattern (Na *et al.*, 1992)
First mode velocity: C_1=3.22 m/sec
Second mode velocity: C_2=1.73 m/sec

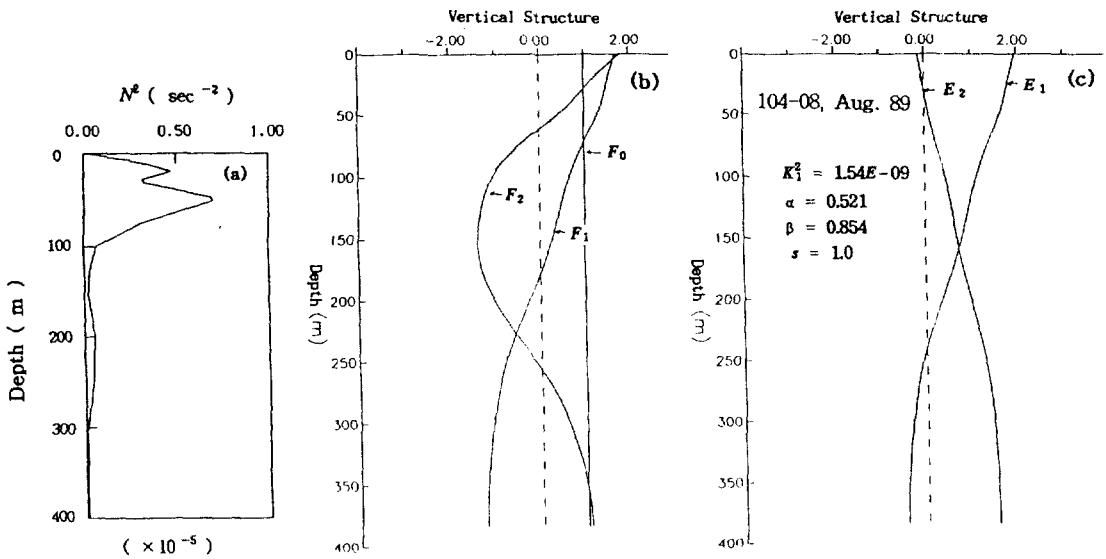

Fig. 2. The vertical structure of the quasi-geostrophic model. (a) The vertical profile of N^2 associated with the realistic stratification in the East Sea. (b) The first three vertical modes: F_0 is barotropic, F_1 and F_2 are the first and second baroclinic. (c) The vertical EOF structure associated with the dynamic modes. $E_1(z)=\alpha+\beta F_1(z)$, $E_2(z)=-\beta+\alpha F_1(z)$.

showed the corresponding eigenvectors of the first two modes for each of the variables more than 90 percent. Mode E_1 has its dominant kinetic energy (KE) above 500 m, while mode E_2 has its dominant KE below 500 m. The vertical EOF modes associated with dynamic modes are shown in Fig. 2c. We decompose the streamfunction Ψ into vertical EOF modes:

$$\Psi = \Psi_1(x,y,t)E_1(z) + \Psi_2(x,y,t)E_2(z) \tag{2.1}$$
$$E_1(z) = \alpha + \beta F_1(z)$$
$$E_2(z) = (-\beta + \alpha F_1(z))s$$

Where $s=\pm 1$, $\alpha^2+\beta^2=1$, $<E_1^2>=<E_2^2>=1$, $<E_1\ E_2>=0$, and $<\ >$ an inner product of two vectors. α and β are calculated by normalization of the dynamic vertical functions.

The governing equations are the quasi-geostrophic, nonlinear potential vorticity equations for two modes. The quasi-geostrophic assumption implies that the time scale of the flow is large compared to the Coriolis period and the flow is nearly horizontally non-divergent. The analysis we conducted follows closely that of Cumins and Mysak (1988).

(1) (2)

$$\frac{\partial}{\partial t}\begin{bmatrix}\nabla^2\Psi_1\\ \nabla^2\Psi_2\end{bmatrix} - \begin{bmatrix}\beta\\ \alpha s\end{bmatrix} k_1^2\left\{\frac{\partial}{\partial t}(\beta\Psi_1 + \alpha s\Psi_2) + s\,J(\Psi_1,\Psi_2)\right\}$$

(3) (4) (5)

$$+\begin{bmatrix}A_1(\Psi_1,\Psi_2)\\ A_2(\Psi_1,\Psi_2)\end{bmatrix} + J\left(\begin{bmatrix}\Psi_1\\ \Psi_2\end{bmatrix}, f\right) - \begin{bmatrix}E_{1b}\\ E_{2b}\end{bmatrix}\frac{f}{H}J(\Psi_b,h)$$

(6) (7) (8)

$$= \begin{bmatrix}E_{1s}\\ E_{2s}\end{bmatrix}\frac{f}{H}W_e - \begin{bmatrix}E_{1b}\\ E_{2b}\end{bmatrix}\frac{r}{H}\nabla^2\Psi_b + A_h\nabla^4\begin{bmatrix}\Psi_1\\ \Psi_2\end{bmatrix} \tag{2.2}$$
$$\Psi_b = E_{1b}\Psi_1 + E_{2b}\Psi_2$$

where E_{1s} is EOF mode one at the surface, E_{2s} is EOF mode two at the surface, E_{1b} is EOF mode one at the bottom, E_{2b} is EOF mode two at the bottom. The definition of parameters used in this model are given in Table 1. The terms in the equation (2.2) are such that (1) is the local time change of mean relative vorticity tendency, (2) the divergence of mean vorticity tendency, and also includes contributions to mean and eddy vortex stretching tendency, (3) the advection of mean relative vorticity and eddy relative vorticity tendency. (4) the mean advection of planetary vorticity tendency, (5) and (6) give the contribution to the vorticity balance from the external forcing and the topographic vortex stretching tendency. (7) gives the mean contribution from the bottom friction, while (8) represents the lateral friction of mean vorticity tendency. The notations are as follows: H is the depth of water column; J is the Jacobian operator; $f=f_0+\beta(y-y_0)$ is the variable Coriolis parameter (y_0 refers to the mid-latitude of the basin); β is the latitude gradient of f; and W_e is Ekman pumping. Vorticity is dissipated by linear bottom friction with coefficient r, and in each mode, vorticity is dissipated by Laplacian lateral friction with A_h.

The advection terms A_1 and A_2 are as follows:

$$\begin{bmatrix}A_1\\ A_2\end{bmatrix} = \begin{bmatrix}\mu_0\\ \mu_1\end{bmatrix} J(\Psi_1,\nabla^2\Psi_1) + \begin{bmatrix}\mu_1\\ \mu_2\end{bmatrix}(J(\Psi_1,\nabla^2\Psi_2) + J(\Psi_2,\nabla^2\Psi_1)) + \begin{bmatrix}\mu_2\\ \mu_3\end{bmatrix} J(\Psi_2,\nabla^2\Psi_2) \tag{2.3}$$

where

$$\mu_0 \equiv <E_1^3> = \alpha^3 + 3\,\alpha\beta^2 + \beta^3 <F_1^3>$$
$$\mu_1 \equiv <E_1^2 E_2> = \beta(-\beta^2 + \alpha^2 + \alpha\beta <F_1^3>)s$$
$$\mu_2 \equiv <E_1 E_2^2> = \alpha(\alpha^2 - \beta^2 + \alpha\beta <F_1^3>)$$
$$\mu_3 \equiv <E_2^3> = (-\beta^3 - 3\alpha^2\beta + \alpha^3 <F_1^3>)s$$

The model is forced by the inflow through the Korean Strait and by the curl of the surface wind stress. The annual average wind stress curl for the East Sea (Na, *et al.*, 1992) has a positive maximum in the center of the northwestern part and zero at the center of basin shown in Fig. 3. Fig.4 shows variation of volume transport stream function specified along the Korea Strait at 20-day interval. The veloc-

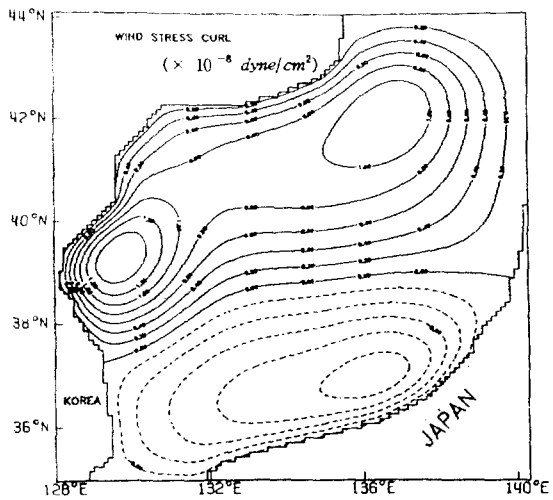

Fig. 3. Annual average wind stress curl used in the model. This structure approximates with two positive maxima in the northern part and near the Wonsan Bay, and the negative curl in the southern part of the East Sea (Na, *et al.*, 1992).

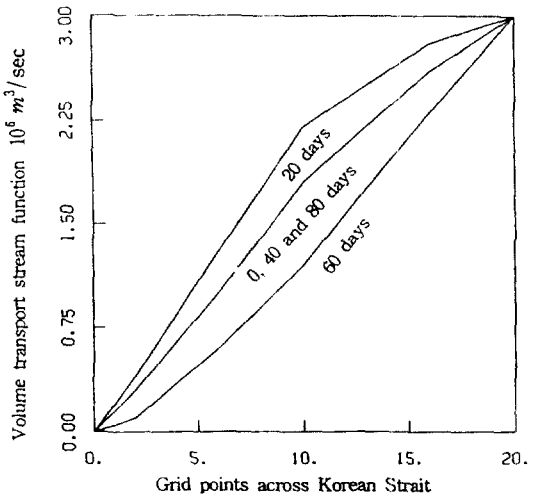

Fig. 4. Volume transport stream function across the Korea Strait at 20 day interval.

ity distribution is varied sinusoidally over a 1-year period, about mean while maintaining a constant 3×10^6 m^3/sec flow. The effect of this variation is to intensify the flow to the west. With little westward intensification, most of warm eddies may not be generated in this experiment. Thus the distribution of the velocity in the inflow seems to be essential in generating the warm eddy. The zero curl line along 38°N is the general boundary between the TWC (Tsushima Warm Current) and the northern cold water gyre. This boundary is represented in this model as the TWC main stream. This structure approximates the horizontal structure of annual average wind curl. The boundary conditions are specified as free slip on walls except the Korea Strait and the Tsugaru Strait. Since the walls are impermeable, the stream function has a constant value along wall. The Japan side wall of the East Sea is chosen, without loss of generality, to have a stream function value of 3.0 sv. The value for the northern wall has a constant value to have a stream function value of zero.

Equations (2.2) are integrated on a realistic basin whose zonal and meridional dimensions are L_x=1000 km and L_y=1000 km, respectively. The square region in Fig. 5 is chosen as a model ocean, which is simplified without losing the characteristic of the bottom topography and coastal geometry. A model depth of 1200m is assumed with a shelf depth of 300m to insure that assumption is satisfied. The numerical instability was eliminated by smoothing the bottom topography with a smoothing function (Shapiro, 1970). The TWC is confined to the upper 300m on average in the Ulleung Basin giving the upstream conditions for local dynamics of the warm eddy. The TWC is driven by an inflow in the Korea Strait and outflow through the Tsugaru Strait. Since the volume transport through the Korea Strait drives the model, the values of ψ across these straits are specified at each time step. The Tsugaru Strait is downstream in the flow and the model is allowed to specify the velocity distribution across this strait. The volume transport in the Korean Strait changes approximately between 2.3 and 3.0 sv.

Equations (2.2) are integrated using centered finite difference representation for spacial derivatives and leap frog differences for time derivatives. To aviod numerical instability, the advection terms are evaluated at the middle time level and the friction terms are evaluated at the oldest time level. The Jacobian term is evaluated with the Arakawa (1966) procedures so that both energy and enstrophy are conserved in the calculation. The wind stress term is

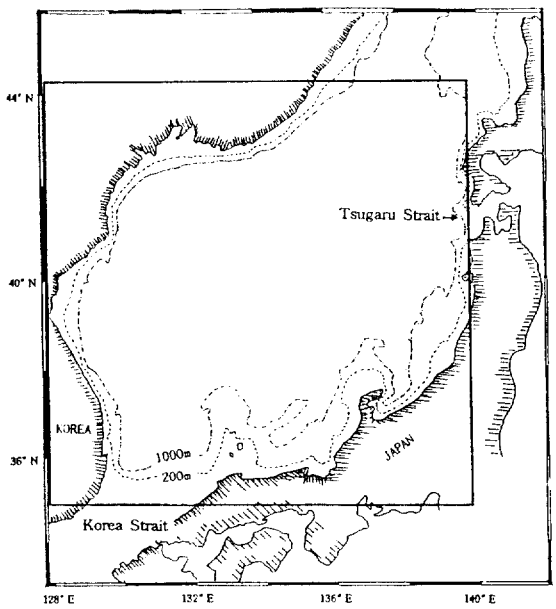

Fig. 5. Bathymetry of the East Sea. The rectangle shows the approximate domain of the numerical model. Results of numerical experiments are presented for the inner square. The locations of the inflow and outflow Straits are also indicated.

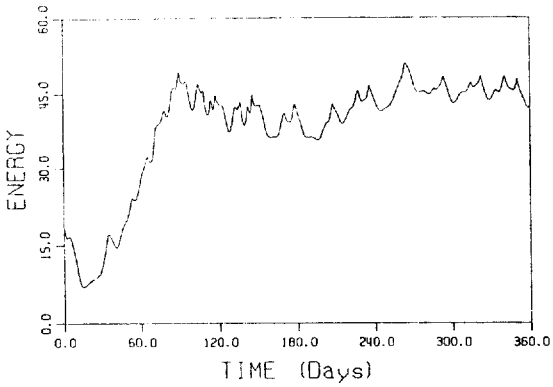

Fig. 6. Time series of the basin averaged total kinetic energy for experiment 4 in Table 2. The units are in J m^{-2} for the kinetic energy.

Table 2. Model experiments discussed in Section 3

Exp#	Differences from standard case flat bottom experiments in Table 1	Figures from these experiments
1	none	Figs. 7a-7e, 9a-9e
2	$A_h=5\times10^6$, 3.0 Sv	
3	$A_h=8\times10^6$, 3.0 Sv	
4	$A_h=1.0\times10^6$, 3.0 Sv	Figs. 8a-8e, 10a-10e
5	$A_h=3.0\times10^6$, $r=5.0\times10^{-8}$	Figs. 11a, 11b, 11c
6	$A_h=3.0\times10^6$, 3.0 Sv Figs 12a topography	Figs. 12b, 12c
7	$A_h=1.0\times10^6$, 2.4 Sv Figs 12a topography	Figs. 13c
8	$A_h=1.0\times10^6$, 1.95 Sv Figs 12a topography	Figs. 13b
9	$A_h=1.0\times10^6$, 1.60 Sv Figs 12a topography	Figs. 13a

calculated at the middle time level. A forward time step is performed every 100 steps to avoid time splitting. The calculation of the stream function is diagnostic, that is, does not involve time derivatives, and is done after the new vorticity value is calculated from evaluation of (2.2).

3. RESULTS OF SIMULATIONS

Effect of Lateral Friction

A set of numerical experiments is carried out in order to test the influence of the western boundary with flat bottom on eddy motion. Variation of the western intensification in the inflow is observed to cause the generation of an anticyclonic eddy and a run of 360 days with input period of 20 days is made that produces the variation from the circulation pattern. The wind stress curl is a maximum in the northwestern center of the basin ocean and zero at the center of the basin. Fig. 6 shows the time-dependent behavior of the basin-averaged total kinetic energy $(\partial\Psi/\partial x)^2+(\partial\Psi/\partial y)^2$ for case 4 in Table 3. This result shows that after about 120 days the model reaches an equilibrium in a statistical sense.

Several coefficients are considered to test the effect of lateral friction on the anticyclonic eddy motion. The basic parameter values for this set of experiments (Table 1) are chosen to correspond to the Ulleung warm eddy. Both bottom and lateral frictions are used in the model and the frictional coefficients range from in the mid to low ends of the acceptable value for eddy motion. For both low and high-friction cases (Case 1 and 4 in Table 2), the northward motions of the warm eddy in the East Sea exhibit the robust features characteristic of this type of eddy resolving model. The stream functions of the first mode for Experiment 1 and 4, shown in

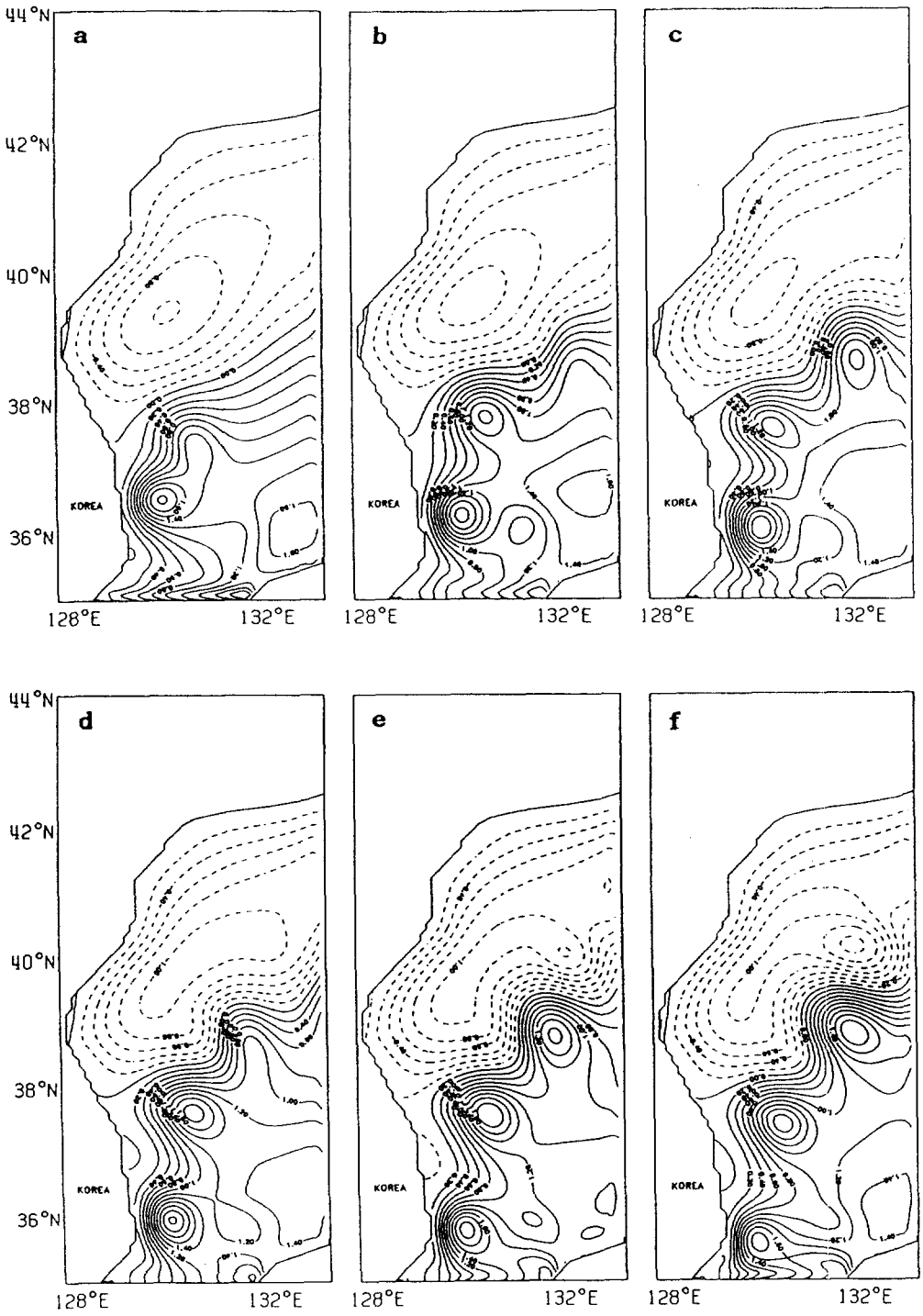

Fig. 7. Instantaneous stream function field every 20 days from day 47(a) to day 147(f) for experiment 1.

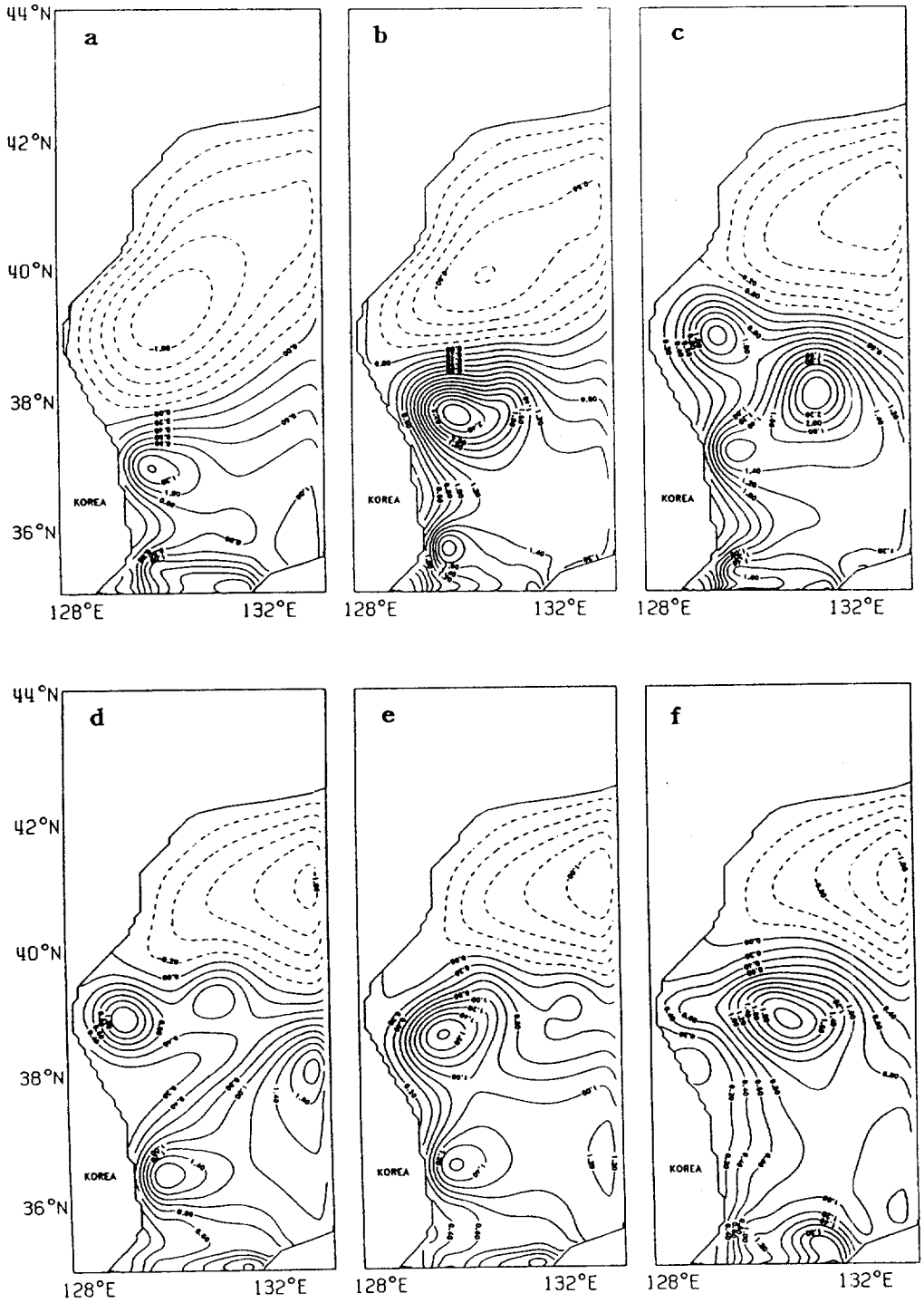

Fig. 8. Instantaneous stream function field every 20 days from day 47 (a) to day 147 (f) for experiment 4.

Table 3. Parameters from experiments

Case	Sv	A_h	Y_e (km)	V_i (cm/s)	V_m (cm/s)	H_m (m)	D_m (km)	R_e	R_b
1	3.0	3.0	220.0	53.0	15.5	337.2	120.5	83.3	0.106
2	3.0	5.0	200.0	53.0	5.1	327.1	85.0	53.0	0.106
3	3.0	8.0	-	53.0	-	-	-	33.1	0.106
4	3.0	1.0	420.0	53.0	23.3	343.3	140.0	265.0	0.106
5	2.4	1.0	400.0	42.5	10.5	338.2	115.0	212.5	0.085
6	1.95	1.0	320.0	34.5	7.5	331.5	100.0	172.5	0.069
7	1.6	1.0	210.0	29.0	3.6	322.9	75.0	145.0	0.058
8	1.5	1.0	190.0	26.5	3.5	322.3	65.0	132.0	0.053
9	1.0	1.0	-	17.7	-	-	-	88.5	0.035
10	1.7	3.0	-	30.3	-	-	-	50.5	0.061
11	2.6	3.0	240.0	45.5	10.5	327.4	115.0	75.8	0.091

R_e Reynolds number $[=V_i L_x A_h^{-1}]$, where L_x is half the width of the Korea Strait.
R_b Beta Rossby number $[=V_i \beta^{-1} L_y^{-2}]$, where L_y is half the distance between the Korea Strait and the Tsugaru Strait.
Y_e Distance from the northern boundary (km) of the eddy centers as they pass a latitude of 38°N along the east coast of Korea.
V_i Maximum current speed (cm/sec) of the inflow.
V_m Maximum current speed (cm/sec) of an eddy measured as the center passes a latitude of 38°N.
H_m Maximum depth in meter of the interface in an eddy as the center passes a latitude of 38°N.
D_m North-south diameter (km) of an eddy measured as the center passes a latitude of 38°N.
A_h Lateral friction coefficient in 10^6 cm^2/sec
Sv Inflow transport in the Korea Strait in 10^6 m^3/sec

Fig. 7 and 8, illustrate time evolution of eddy motion.

Fig. 9 and 10 represent the usual double gyre pattern. The East Sea circulation feeds a narrow western boundary current which, at 38°N latitude, turns into a strong eastward current, penetrating towards the middle of the basin along the line of zero wind stress curl. Eddy moves northward consistent with flat bottom dynamics. The flat bottom case can be easily understood with analytic method as investigated by Smith and Reid (1982); anticyclones over a flat bottom have a tendency to move westward due to nonlinearity. This tendencies happen as the eddy becomes asymmetric through dispersion of its Rossby waves. Since longer wave components have greater westward phase velocity than shorter wave components, dispersion makes steepening of pressure gradients on the trailing side of the eddy. The anticyclonic eddy is developed in the west as the result of the nonlinear advection term and the dispersion mechanism. The warm eddies evolve due to planetary dispersion and lateral friction. As lateral friction decreases slowly with eddy dispersion or decay, northward motion along the east coast of Korea may weaken by the consideration of lateral friction. The southern anticyclonic eddy moves to the north along the western boundary due to nonlinear term, and is subsequently advected by another eddies.

Let us investigate the effect of the lateral friction. The plots of Fig. 9 and 10 illustrate a remarkable difference in the northward penetration scale of eddy between high-friction and low-friction, and that this effect is larger as the value of lateral friction is lower. The northward penetration of the anticyclone eddy is drastically increased by the decrease of the lateral friction. We define this scale, Y_e as the distance from the Korea Strait. This length is taken as the maximum distance over which eddies move northward from the Korea Strait. Table 3 shows the northward distance Y_e obtained from the different experiments; Y_e is almost 90% larger in Case 4 with $A_h=1.0\times10^6$ cm^2/sec than in Case 1 with $A_h=3.0\times10^6$ cm^2/sec.

The instantaneous stream functions of the first mode shown in Fig. 9 also reveal interesting features. In $A_h=3.0\times10^6$ cm^2 s^{-1} case, besides the decreased distance of northward motion, the eddy activity develops into meandering in comparison with the case $A_h=1.0\times10^6$ cm^2 s^{-1}. In both experiments,

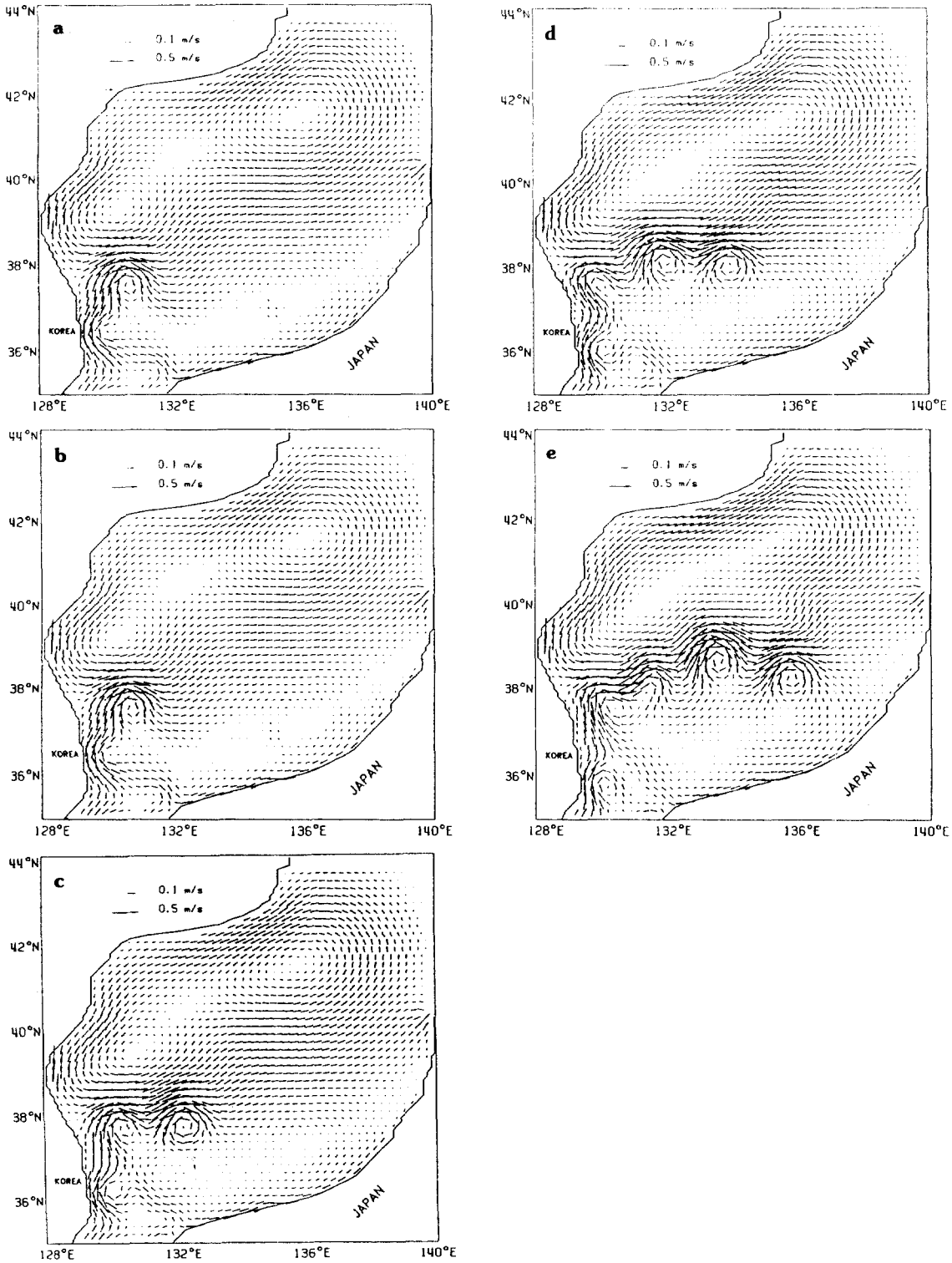

Fig. 9. Instantaneous velocity field every 20 days from day 64(a) to day 144(e) for a high lateral friction experiment (A_H=3.0× 10^6 cm^2/sec); (a) Day 64, (b) Day 84, (c) Day 104, (d) Day 124 and (e) Day 144.

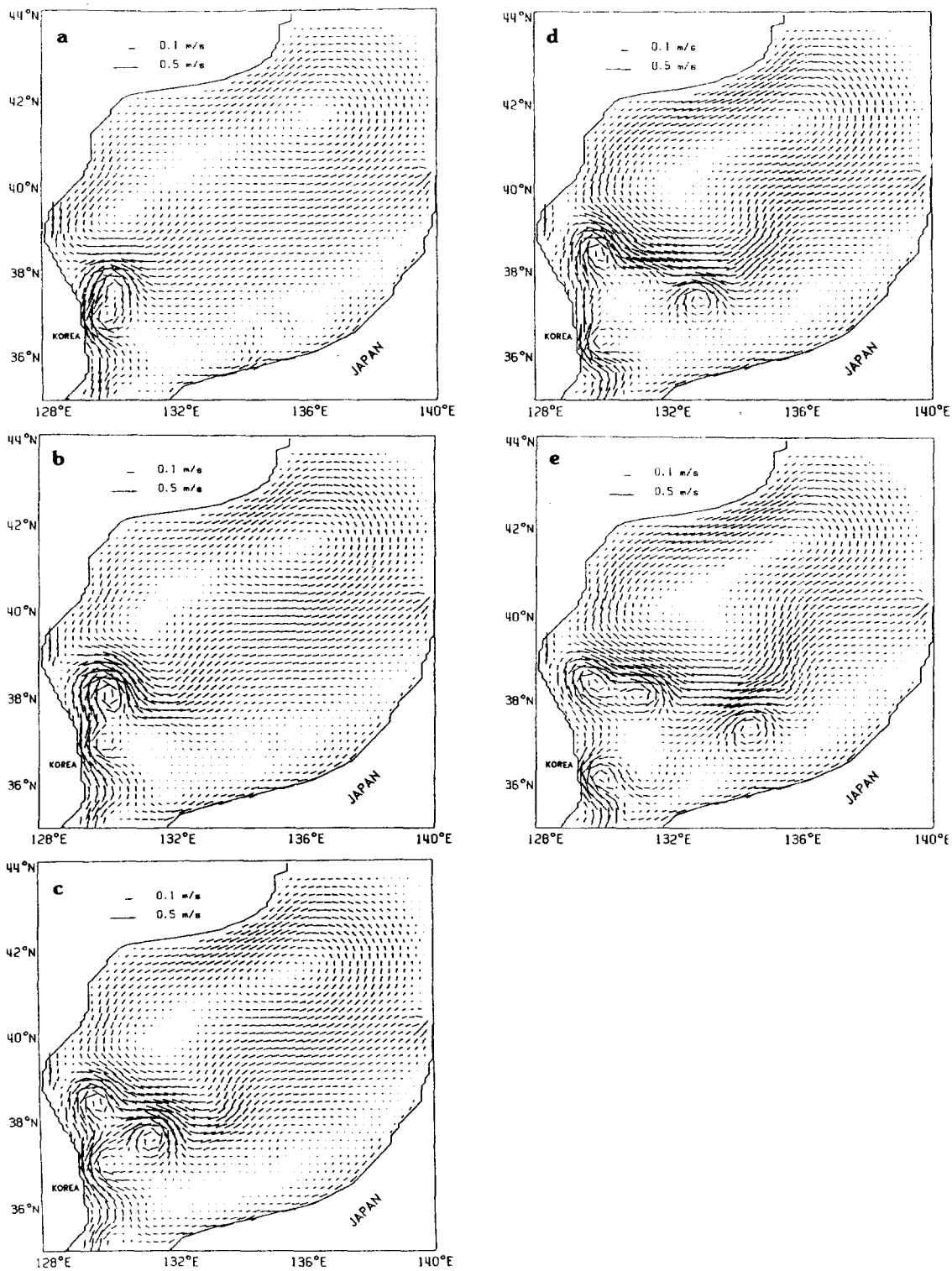

Fig. 10. Instantaneous velocity field every 20 days from day 64(a) to day 144(e) for a low lateral friction experiment (A_H=1.0×10^6 cm^2/s)$^{-1}$; (a) Day 64, (b) Day 84, (c) Day 104, (d) Day 124 and (e) Day 144.

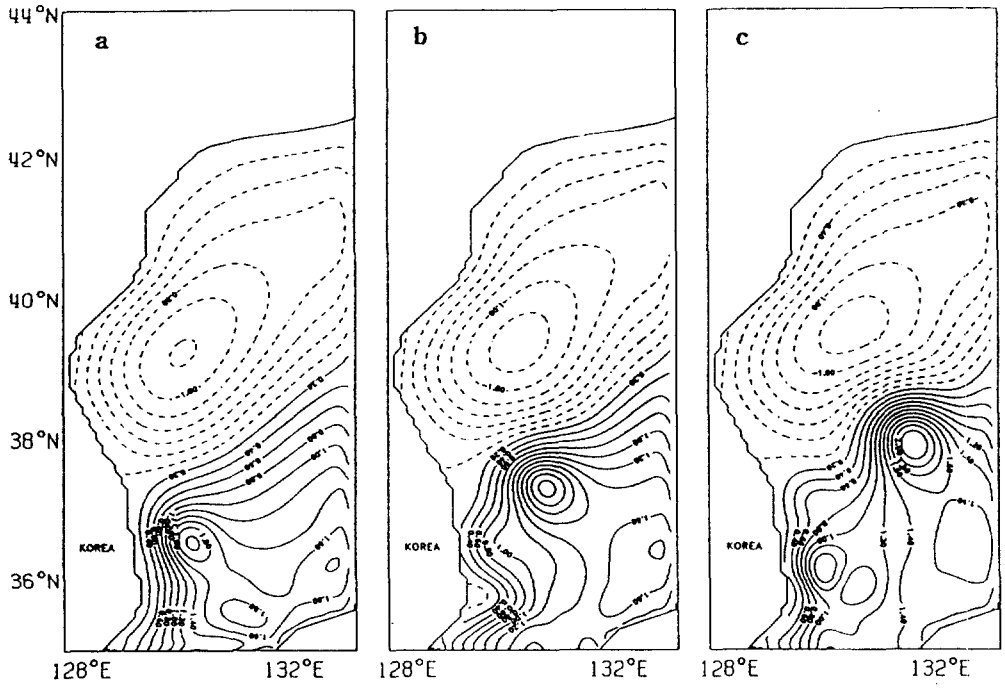

Fig. 11. Instantaneous velocity field every 10 days from day 50 to day 70 for a bottom friction experiment ($r=5.0\times10^{-8}$ s^{-1}).

formation of warm eddy has been observed, and most eddies are generated as the inflow leaves the Korea Strait. In low lateral friction case, the warm eddies are more sharply delineated and their lifetime is several times longer than in high lateral friction. This is because when lateral friction is high, the eddies are more often absorbed by the meandering of the Tsushima Warm Current. We thus expect the eddy-mean flow interaction to be quite different in both experiments.

In Rossby number (R_b) experiments (Table 3, case 5-6), the increase of Y_e due to the increase in R_b is nearly 25%. To sort out the effects of dissipation and inflow transport, we now consider experiments with low lateral friction. In the parameter range used in the present study, reducing effect appears to be quite different in low lateral friction cases. In the weak R_b case, the reduction of the lateral friction seems to have little effects on the northward motion; Y_e is almost identical in R_b=0.058 and R_b=0.053.

The combined effects of the R_e and R_b on the eddy motion are summarized in Table 3. Comparision of R_b=0.085 with R_b=0.069 shows that the increase in R_b produces a large increase of the northward distance of the warm eddy. Comparision of R_b =0.106 and R_b=0.085 indicates that an increase in R_b seems to have little influence on the northward distance of the warm eddy. But the comparision between R_e and R_b indicates that an increase of R_b drastically increases the strength of circulation. This demonstrates the importance of the contribution of the inflow transport in determining the northward motion of the warm eddy.

Effect of Bottom Friction

The distance of the penetration pattern achieved with high-friction depends on parameters such as the coefficient of bottom friction. Fig. 11 shows the results of an experiment where the coefficient of bottom friction is 50% smaller ($r=5.0\times10^{-8}$ s^{-1}) than that of the standard case from day 50 to 70.

The reduction of bottom friction seems to have lit-

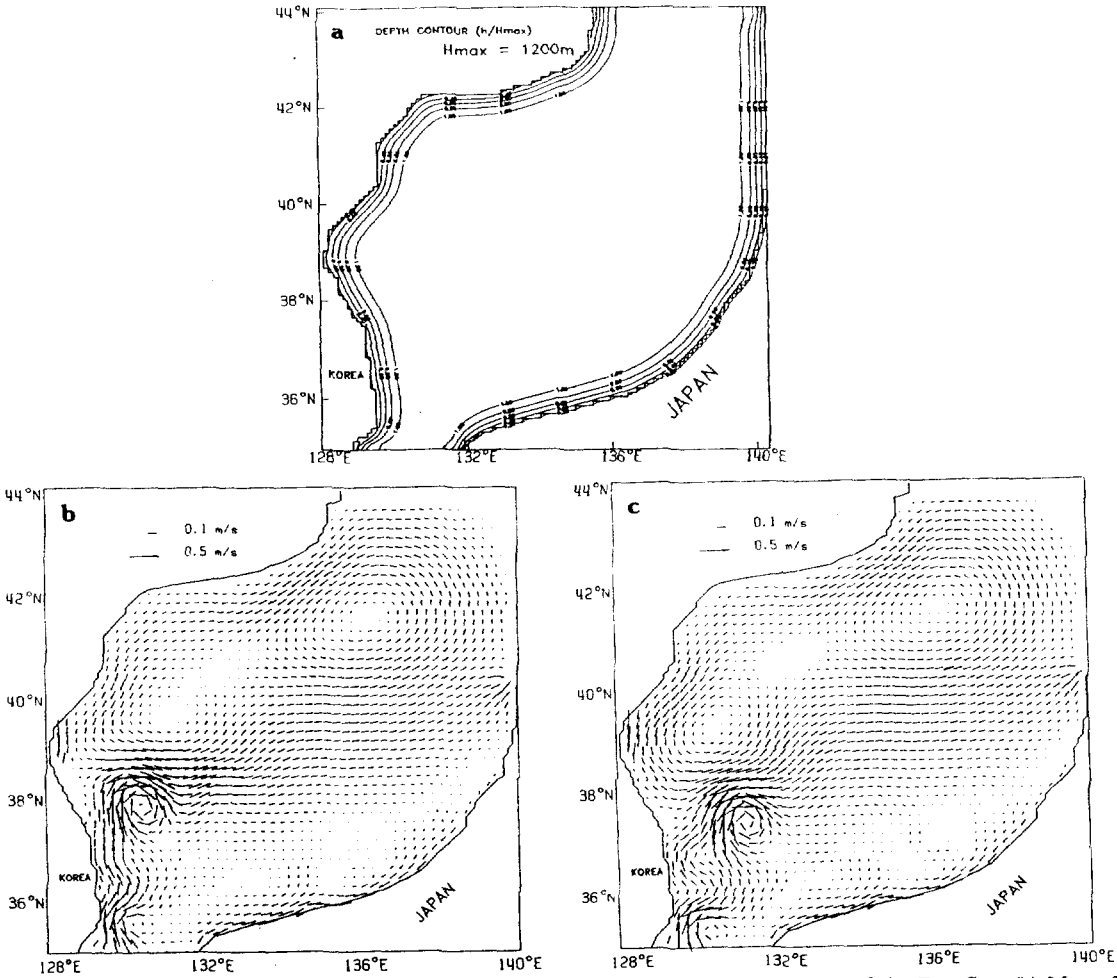

Fig. 12. Results for the effects of bottom topography experiments. (a) bottom topography of the East Sea. (b) Map of velocity field for a narrow slope experiment at day 64. (c) Map of velocity field for a wide slope experiment at day 64.

tle effect on the northward penetration of the warm eddy, but the maximum velocity of the warm eddy is considerably stronger. Speed in the Tsushima Warm Current increases by 25%. This has to be compared with Fig. 10, where a stronger inflow produced eddy speeds 50% larger than those in the standard case of Fig. 9, but did not show the same effect on the distance of northward penetration as the small bottom friction.

The growth of the anticyclonic eddy with lower values of bottom friction can again be explained in terms of vorticity. The scale of model eddy size is determined by lateral friction because the influence of bottom friction was chosen relatively small. Quantitatively, bottom friction experiments appear to be less sensitive to change in eddy size. Our results is that the bottom friction coefficient modifies the role of lateral friction in its control of the balance between inertia and instability processes. The bottom friction has two opposite effects on the northward motion of the warm eddy: it has a global damping effect on the eddy motion and prevents inertia to bring the eddy across the East Sea, but it also damps the nonlinear effects. Hence almost everywhere in the East Sea bottom friction is an important sink for vorticity. So the change in bottom

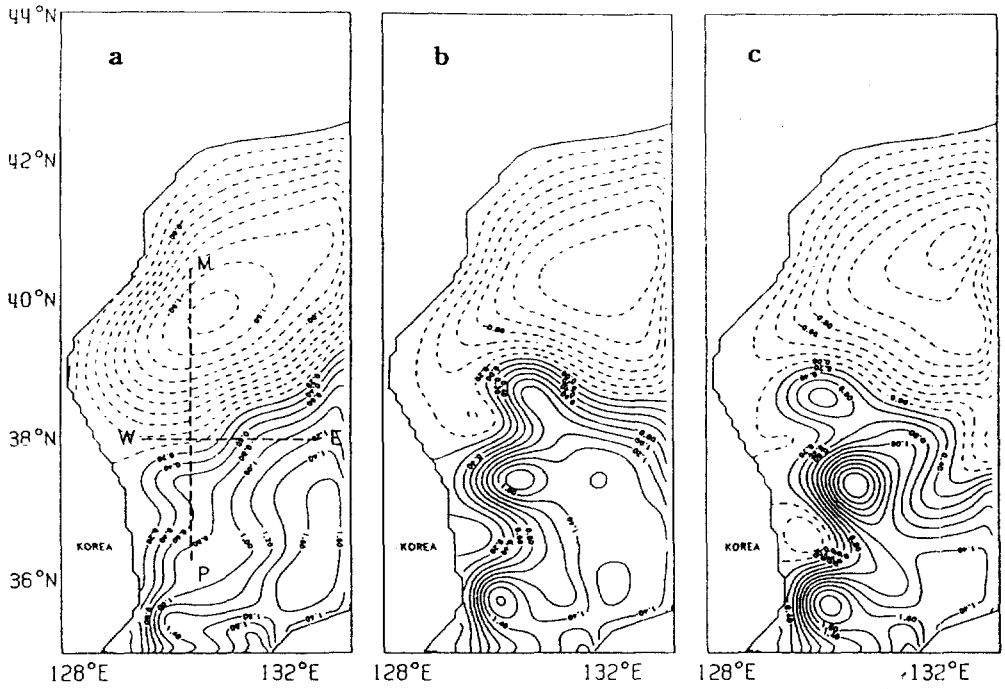

Fig. 13. Instantaneous stream function field at day 105 for the mode one. (a) R_e=145.0 and R_b=0.058, (b) R_e=172.5 and R_b=0.069, (c) R_e=212.5 and R_b=0.085.

friction has considerable effects in the interior of the East Sea.

Bottom Topographic Influences

Fig. 12a shows that the bottom topography of the East Sea used in this model, which varies dramatically over the basin and is deeper than 1000m in the western side. From simple scaling of the depth averaged vorticity equation (2.2), it can be shown easily that bottom slopes result in a larger contribution of the topographic vorticity tendency than the planetary vorticity tendency to the vorticity equation. The bottom topography system is much more difficult to discuss because the western boundary with topography must be considered. Along the east coast of Korea the topography β_T is almost balanced by lateral friction because β_T is two orders of magnitude greater than planetary β. For eddies dispersing over topography, the nonlinear tendencies are a function of time (Smith, 1986). For an initially strong anticyclone, inshore directed propagation can occur. For intermediate strength anticyclones one might anticipate a balance between the nonlinear term and the β_T effects which would result in a stationary anticyclone over topography. As nonlinearity decreases with eddy dispersion, southward motion along the topographic slope may be weakened by topographic Rossby wave conception. If the lateral friction is included over topography, the eddies may propagate northward with motion controlled by the western boundary. This paper will test northward motion for anticyclone eddies associated with their lateral coefficient value. We have demonstrated the crucial role of topography beta (β_T) in the eddy motion process.

We will investigate the additional influence of the topography. Further, it is likely that the northward penetration of eddy observed in the flat bottom experiment is considerably modified by the bottom topography. To show the consequences of this effect on bottom topography; the width of bottom slope was changed in the following set of experiments. At a slim slope (about 50 km of slope width, Fig. 12a)

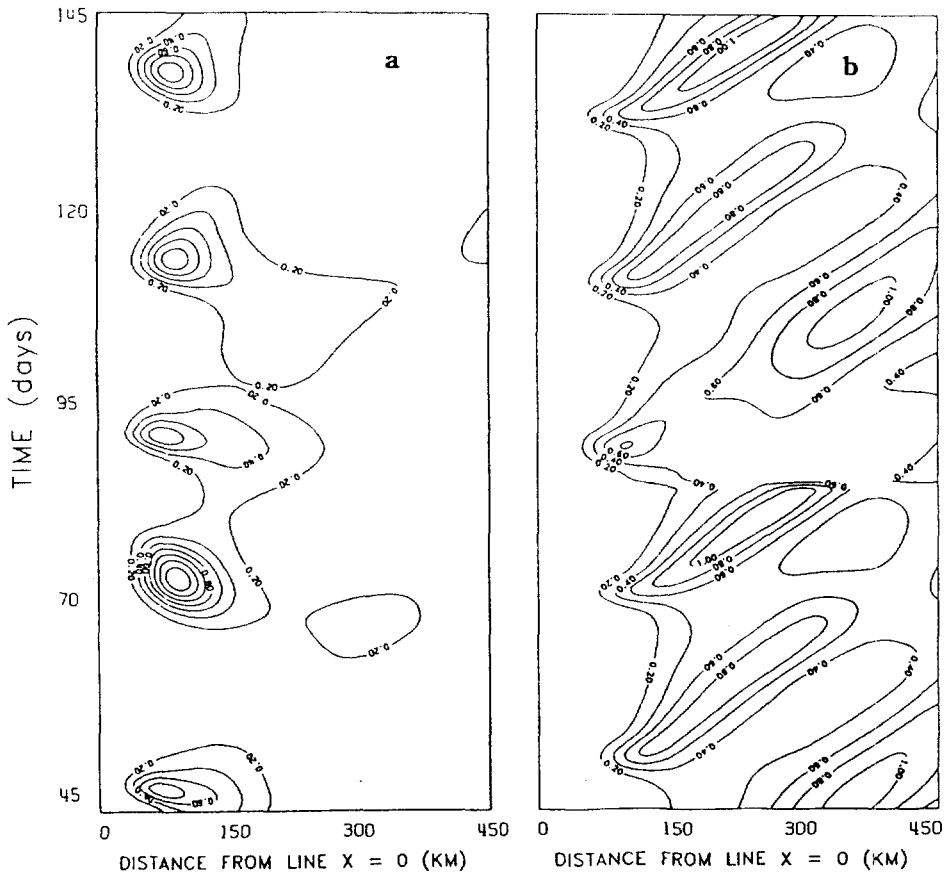

Fig. 14. Time history of potential energy along the line WE in Fig. 13a. (a) flat topography, (b) with bottom topography.

the warm eddy moves northward in the way shown in Fig. 12b. If the width of the bottom slope is increased from 50 km to 100 km, the velocity distribution forms an anticyclonic circulation that leaves the coast before the warm eddy can reach the latitute of 38°N as shown in Fig. 12c. A further increase in the width of the bottom slope does not result in a significant change of the warm eddy's size.

If the bottom slope of Fig. 12a is used for different values of the inflow forcing as shown in Fig. 13a-c, the warm eddy moves down along the coast with increasing strength of the inflow transport. Fig. 13 shows the streamfunction field at day 105 for mode one. The course of the warm eddy becomes more eastward, disguising the early penetration to some degree, and the size of the warm eddy increases. Both the warm eddy's radius and the distance of the penetration from the Korea Strait are based on the inertial length scale ($L=(v/\beta)^{1/2}$) from Table 2 of Hurlbert and Thompson (1980), the same ones they used in a similar hypothesis testing.

With increasing strength of the inflow transport the warm eddy grows in size and its radius is again determined by the Rossby radius of deformation. There is a marked difference, however, in that time the penetration distance of the warm eddy moves northward with larger Rossby numbers. For weak inflows (Fig. 13a) the warm eddy is not able to reach the latitute of 40°N; in fact, it turns immediately into the Ulleung Island at the latitute of 38°N. For strong flow transport (Fig. 13c) the warm eddy reaches almost 39°N. At a high Rossby number (Fig. 13c) the eddy is able to reach the northern part as a con-

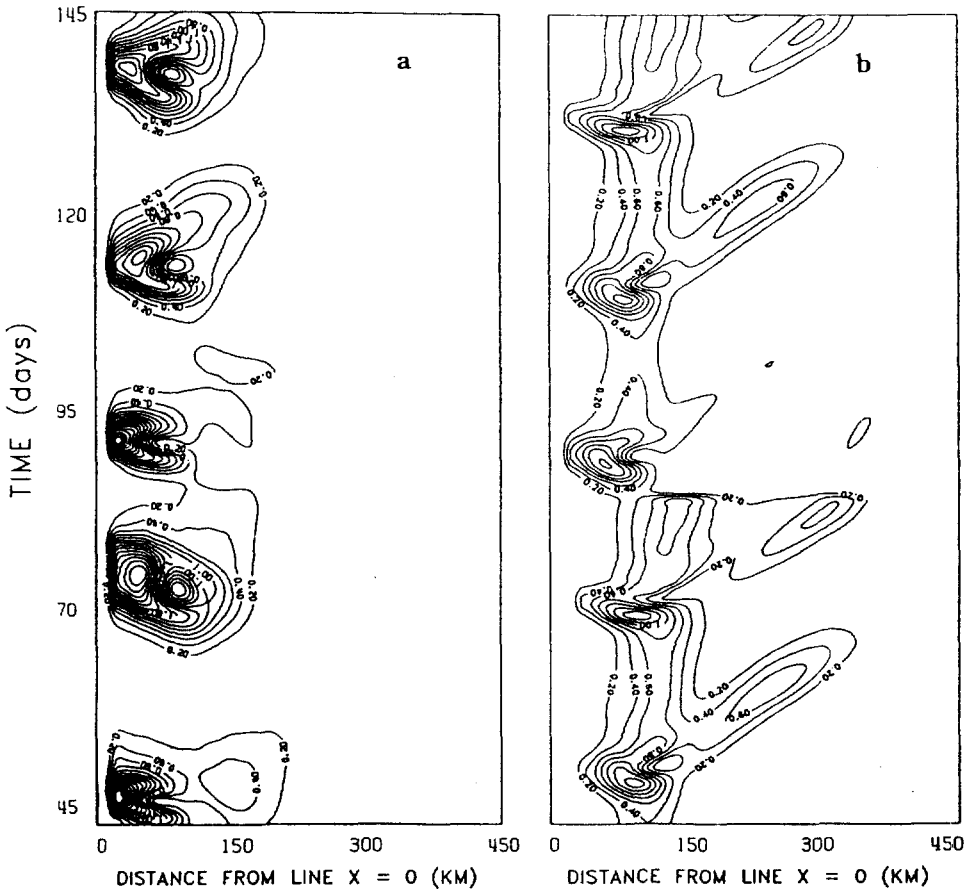

Fig. 15. Time history of kinetic energy along the line WE in Fig. 13a. (a) flat topography, (b) with bottom topography.

centrated jet. However, there are two factors that may be responsible for the dependence of the distance of the penetration pattern. As already mentioned, one is the width of the continental shelf and slope, which might have some kind of blocking effect; the other is the strength of the inflow transport.

To illustrate topographic control on the two-EOF modes system, we designed a standard experiment with bottom topography. The deepest water was 1000m in each case, and a 3.0 sv inflow transport was applied with a given cross stream inflow profile. Fig. 14 and 15 are the phase diagram (time history) for the eddy kinetic energy and potential energy from day 45 to day 145 along the line WE of Fig. 13a. This phase diagram shows clearly the periodicity and propagation of the warm eddy. Although each experiment was forced with the same inflow transport in the upper layer, it is clear that the energy of the warm eddy is remarkably different in the two cases. Loss of energy to the deep water through a baroclinic instability is weak in the flat bottom model. Consequently, the warm eddy maintains its intensity as it approaches the western boundary. The short period (20 days) of inflow transport in the two-modes with bottom topography results in a consequence of the loss of energy from the upper to the lower layer which tends to weaken the warm eddy. As seen Fig. 16, it shows the phase diagram for the nonlinear term (A_1 term) of equation (2.2) from day 45 to day 145 along the line WE in Fig. 13a. Examining carefully Fig. 16, one can see that local high values occur when the warm eddy is shift-

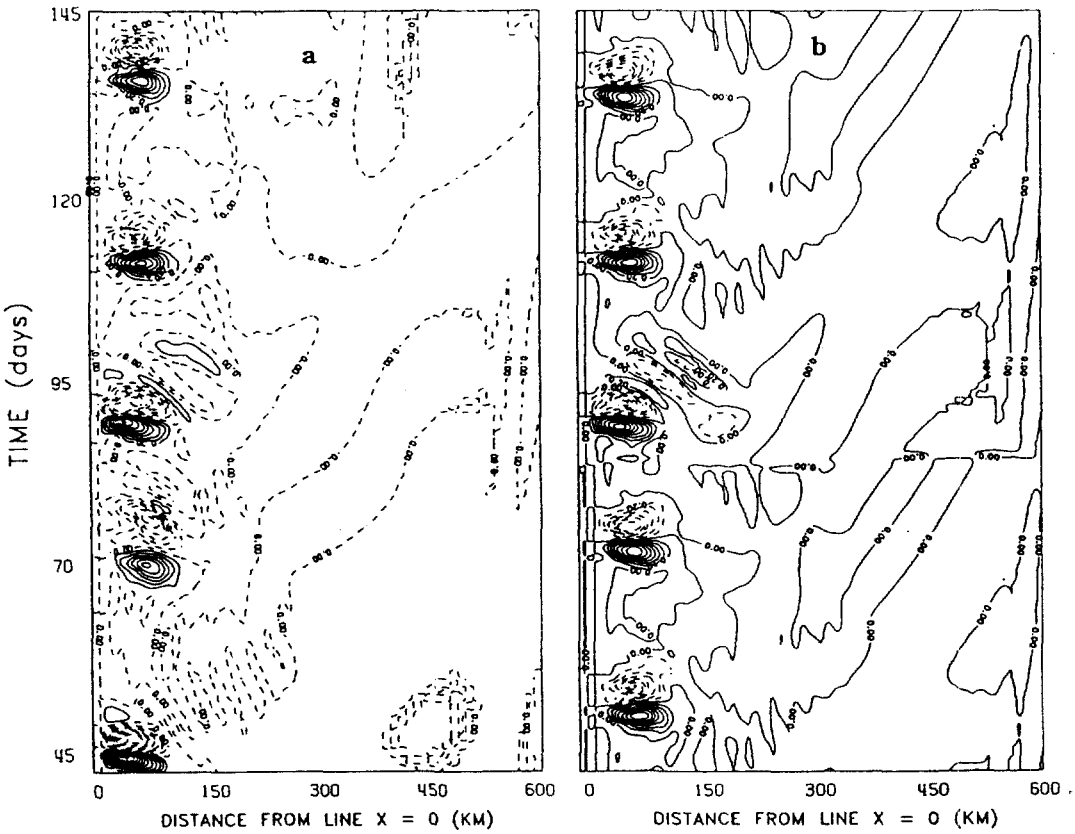

Fig. 16. Time history of nonlinear term along the line WE in Fig. 13a. (a) flat topography, (b) with bottom topography.

ed to the west. This is an evidence of baroclinic instability that may be one of the mechanism for the variability of the meandering jet. Our results are consistent with the fact that the inflow transport period becomes shorter in the experiment with greatest energy loss from the TWC to the lower layer and longest with no transfer of energy to the lower layer.

Since inclusion of bottom topography significantly reduces the transfer of energy to the deep water compared to the flat-bottom model, our use of the two-modes model with topography, is both useful and in some ways more realistic than the use of a two layer flat-bottom model.

4. CONCLUSIONS

The interaction of Tsushima Warm Current eddies with a lateral boundary in the East Sea has been examined with a two-EOF numerical model. Warm eddy can be induced by the inflow through the Korean Strait. Variation of the western intensification in the inflow is observed to cause the generation of an anticyclonic eddy, and a run of 360 days with input period of 20 days is made to produce the changes in the circulation pattern. It is found that the model can simulate observed features of the eddy when model parameters for the East Sea are used, including the size, movements and thickness of the warm eddies. We have also found that time variations in the inflow are required for the eddy generating to occur at a realistic period.

Our numerical results have confirmed the importance of the lateral friction on eddy motions. They show that the northward penetration of the anticyclonic eddy is drastically increased by the decrease of the lateral friction. The eddy penetration

can be prevented by reducing the Reynolds number (R_r) sufficiently. Those effects, which are already significant when the Rossby number (R_b) is high, are quantitatively more important when R_b is high. The bottom friction does not modify the eddy driven circulation by more than 10%. Experiments using this model show that while the solution depends on the shape of topography, it is relatively insensitive to bottom friction. Hence the bottom friction is an important sink for vorticity almost everywhere in the circulation of the East Sea . The change in a bottom friction (r) shows considerable results in the interior of the circulation.

We have demonstrated the crucial role of topographic effects in the eddy motion process. It is likely that the baroclinic instability observed in the flat bottom experiment is considerably modified by the bottom slope, since the bottom slope significantly reduces the transfer of energy to the deep water compared to the flat-bottom model.

ACKNOWLEDGEMENTS

KSL was supported by the Postdoctral Program for the Research Institute of Basic Sciences, Seoul National University in 1993-1994 and, in part, by the Basic Science Research Institute Program, Ministry of Education (1993). KK appreciates the support from the Korea Science and Engineering Foundation during 1993-1995. This study was also supported in part by the Basic Science Research Institute Program, Ministry of Education (BSRI 95-5406).

REFERENCES

An, H. S., K. S. Shim and H. R. Shin, 1994. On the warm eddies in the southwestern part of the East Sea. *J. Oceanol. Soc. Korea,* **29**: 152-163.

Arakawa, A., 1966: Computational design for long-term numerical integration of the equations of fluid motion. Part I, *J. Comp. Phys.,* **1**, 119-143.

Cummins, P. F. and L. A. Mysak, 1988: A Quasi-geostrophic circulation model of the northeast pacific. Part I: A preliminary numerical experiment. *J. Phys. Oceanogr.,* **18**, 1261-1286.

Holland, W. R. and L. B. Lin, 1975: On the generation of mesoscales eddies and their contribution to the oceanic general circulation. I. A preliminary numerical experiment. *J. Phys. Oceanogr.,* **5**, 642-657.

Hurlbert, H. E. and J. D. Thompson, 1980: A numerical study of Loop current intrusions and eddy shedding. *J. Phys. Oceanogr.,* **10**, 1611-1651.

Ichiye, T. and K. Takano, 1988: Mesoscale eddies in the Japan Sea. *La mer,* **26**, 69-75.

Isoda, Y., M. Naganobu, H. Watanabe, and K. Nukata, 1992: Horizontal and vertical structures of a warm eddy above the Yamato rise. *Research of the ocean,* **1**, 141-151.

Isoda, Y. and S. Saitoh, 1993: The northward intruding eddy along the east coast of Korea. *J. Oceanogr. Soc. Japan,* **49**, 443-458.

Kang, H. E. and Y. Q. Kang, 1990: Spatio-temporal characteristics of Ulleung warm lens. *Bull. Korean Fish. Soc.,* **23**, 407-415.

Kim, H. R., 1991: The vertical structure and temporal variation of the intermediate homogeneous water near Ulleung island., Master of Science, Seoul National University, (in Korean) pp 84.

Kim, K., K. R. Kim, J. Y. Chung, H. S. Yoo and S. G. Park, 1991: Characteristics of physical properties in the Ulleung Basin. *J. Oceanol. Soc. Korea,* **26**, 83-100.

McWilliams, J. C. and G. R. Flierl, 1979: On the evolution of isolated nonlinear vortices. *J. Phys. Oceanogr.,* **9**, 1155-1182.

Na, J. Y. and B. H. Kim., 1990: A laboratory study of formation of 'the Warm Core' in the East Sea of Korea. *Bull. Kor. Fish. Soc.,* **22**, 415-423.

Na, J. Y., J. W. Seo and S. K. Han., 1992: Monthly-mean sea surface winds over the adjacent seas of the Korea peninsular. *J. Oceanol. Soc. Korea,* **27**, 1-10.

Seung, Y. H., S. Y. Nam and S. Y. Lee., 1990: A combined effect of differential cooling and topography on the formation of Ullung Warm Eddy. *Bull. Kor. Fish. Soc.,* **22**, 375-384.

Shapiro, H., 1970: Smoothing, filtering, and boundary effects. *Reviews of Geophysics and Space Physics,* **8**, 359-387.

Shin, H. R., S. K. Byun, C. S. Kim, S. C. Hwang and C. W. Shin, 1995: The characteristics of structure of warm eddy observed to the Northwest of Ulleungdo in 1992. *J. Oceanol. Soc. Korea,* **30**, 39-56.

Smith, D. C., 1986: A numerical study of Loop current eddy interation with topography in the western Gulf of Mexico. *J. Phys. Oceanogr.* **16**, 1260-1272.

Smith, D. C. and R. O. Reid, 1982: A numerical study of non-frictional decay of mesoscale eddies. *J. Phys. Oceanogr.,* **12**, 244-255.

Smith, D. C. and J. J. O'Brien, 1983: The interaction of a two layer isolated mesoscale eddy with topography. *J. Phys. Oceanogr.* **13**, 1681-1697.

Sturges, W., J. C. Evans, S. Welsh and W. Holland, 1993: Separation of Warm-Core Rings in the Gulf of Mexico. *J. Phys Oceanogr.,* **23**, 250-268.

Tameishi, H., 1987: Application of satellite NOAA image for fisheries. *Bull. Japan. Soc. Sci. Fish.*, **51**, 238-244.

Tang, T. Y. and R. H. Weisberg: Vertical structure of low frequency variablity in the eastern equatorial pacific ocean. *J. Phys. Oceanogr.*, **18**, 1009-1019.

Wert, R. T. and R. O. Reid, 1972: A baroclinic prognostic numerical circulation model. Contributions to the Physical Oceanography of the Gulf of Mexico, Vol. II. 177-210.

Accepted January 15, 1996